Impact of Structural Flexibility on Loads on Tidal Current Turbines

Matthias Arnold[#1], Frank Biskup[*2], Po Wen Cheng[#3]

[#]*Stuttgart Wind Energy (SWE),University Stuttgart*
Allmandring 5b, 70569 Stuttgart, Germany
[1]Arnold@ifb.uni-stuttgart.de
[3]Cheng@ifb.uni-stuttgart.de

[*]*Voith Hydro Ocean Current Technologies GmbH & Co. KG*
Alexanderstr. 11, 89522 Heidenheim, Germany
[2]Frank.Biskup@voith.com

Abstract **In the development of tidal current turbines there are two common approaches regarding the required level of detail for load simulations. Those two are either to simulate the pressure field in detail with computational fluid dynamics (CFD) and assume a rigid geometry or to use a high fidelity structural model and simulate the hydrodynamic blade loads with the semi-empirical blade element momentum theory.**

Within the present research this simplification and the impact of fluid-structure-interaction (FSI) on the loads on tidal current turbines are analysed. Based on coupled CFD and multibody simulations the FSI is simulated for the Voith HyTide®1000-13 turbine. This method allows taking the detailed structure of the full turbine into account, while also simulating the detailed pressure field.

Transient simulations of a representative point of operation are performed taking the structural flexibility of the tower, rotor blades, drivetrain and other components into account. This comparison is used to quantify the individual and combined effect of flexibilities on the loads and performance. Therefore, the Voith HyTide®1000-13 turbine is simulated within this research in varying levels of detail to analyse the required level of modelling detail for load simulations of tidal current turbines and increases the understanding of fluid-structure-interaction in tidal current turbine applications.

Keywords **Tidal Current Turbine, Fluid-Structure-Interaction (FSI), Rotor-Stator-Interaction, Transient Rotor Hydrodynamics, Computational Fluid Dynamics (CFD), Multibody Simulation (MBS)**

I. Introduction

The required level of detail in simulations of tidal current turbine varies highly on the desired information to gain. For stochastic and fatigue analysis models simplified to the bare essentials are used, e.g. blade element momentum theory (BEMT) and linearized structural models, [10]. This approach was adapted from wind turbine technologies, where this level of detail is of acceptable accuracy for almost any question, [15].

However, as shown by e.g. [3], [9] BEMT is not valid for tidal current turbines in every case and subsequently computational fluid dynamics (CFD) became common practice, [19]. This direction of increased physical information output and reliability of the models continues in the next step with including the structural responses to the detailed fluid model. The combined hydrodynamic and structural model can then be used to conclude on the hydro-elastic behaviour of the turbine with a fluid structure interaction (FSI) simulation.

This FSI method was initiated with combined methods of BEMT and finite element methods (FEM), [25], and extended to coupled CFD and FEM, [14], [16]. With the rising availability of computational resources this latter approach is recently gaining momentum. However, the application is still limited to either uni-directional weak couplings, [12], [23], or single flexible components of the turbine, e.g. the rotor blade, [7], [18], [20], or the tower, [11].

The here presented research steps in at this point. More and more detailed models are no more able to simulate fatigue and stochastic loads due to the increased computational effort. However, they can be used to answer, which components are relevant for the hydro-elastic behaviour of the tidal current turbine, an essential information for the design of any simplified model.

Therefore based on the method of coupled simulations of CFD and multibody systems (MBS), [4], a detailed structural model of the Voith HyTide®1000-13 turbine is set up and simulated for a deterministic load case scenario. During the simulations the level of detail of the structural model is systematically increased to evaluate the impact on the hydro-elastic behaviour of the system for each component of the turbine.

These results can then be fed back into the simplified methods and therefore serve as a basis for models with increased reliability able to simulate fatigue and stochastic loads with reasonable effort, e.g. [6].

II. Simulation Model

As shown by [3], the hydrodynamics of a tidal current turbine are highly complex and simplified methods can't be used to simulate these in detail, e.g. downstream operation with rotor-tower wake-interaction. Also the effect of added mass is difficult to account for, as multiple objects (tower, nacelle, blades, etc.) intersect. The usual approach of modelling the geometry with non-interfering thin slices to calculate the added mass, the slender body theory [17], is

subsequently not applicable here. Therefore the hydro-dynamics are simulated with a CFD-model, which contains all required details inherently.

For the structural representation of the turbine a model using FEM could be set up based on the full geometric details as shown by [13], [21] and [25]. However, this would result in a very detailed model and lead to high computational costs. Also the application of the FEM model relies on the geometric details, which might not be all available. Therefore the structural model is set up as a multibody system (MBS) and stripped down to the bare requirements to the model for the hydro-elastic simulations.

Those two models are then coupled using a fluid-multibody-interaction (FMBI) method, resulting in a sophisticated model suitable for efficient simulations of the hydro-elasticity.

A. CFD-Model

The hydrodynamics are simulated using computational fluid dynamics (CFD) based on the model developed by [2]. This model is set up in the finite volume URANS CFD code Ansys CFX, [1], using the SST-turbulence model. The basic assumptions regarding simplification of the geometry, cf. Fig. 1, time resolution ($dt \mathrel{\widehat{=}} \Delta\varphi = 2°$), numerical modelling, boundary conditions, etc. are maintained from [2]. This setup has been validated based on full scale prototype measurements by [24].

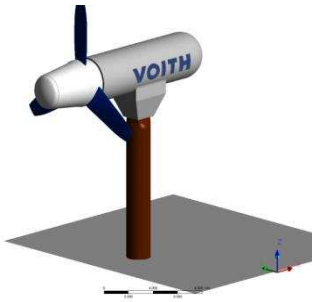

Fig. 1 Simplified geometry for CFD analysis

The basic mesh layout consists of four sections, Fig. 2. In comparison to [2] the grid resolution was reduced to $3.6 \cdot 10^6$ hexahedral elements using an analysis of the flow patterns observed by [3], while increasing the element quality. With this grid the numerical damping for effects like the tip vortex is increased, however a grid study showed negligible impact to the loads and integral properties. For brevity this study is not detailed here.

For the implementation of the FMBI-method two additional changes to the grid are required. Each surface has to be split into regions as will be shown below, Fig. 3, and for a bidirectional coupling the mesh motion has to be activated. The mesh motion can hereto be split into two groups, the volume motion and the prescribed surface motion.

For the volume grid motion the built in algorithms of CFX are applied with increased grid stiffness near boundaries and an adapted displacement diffusion scheme, [1], for increased stability. In vicinity to the rotor blades a protective volume, cf. [4], approx. half the chord length in each direction has been included. This volume is following the prescribed motion from the FMBI surface coupling to prevent quality degradation of the boundary grid. The surface grid motion is directly calculated with the transformation algorithms of the FMBI method.

Special attention was required for the rotor stator grid interface (GGI), as the 2 sides need to slide on each other accordingly to the rotor rotation, but must not detach. Therefore the nacelle motion at this location was applied to the central region ($r < 3m$) and blended over to 0 at the outer region ($r > 9m$), Fig. 4. This method was also applied to the ground near tower bottom to prevent a detachment here due to the ground flexibility.

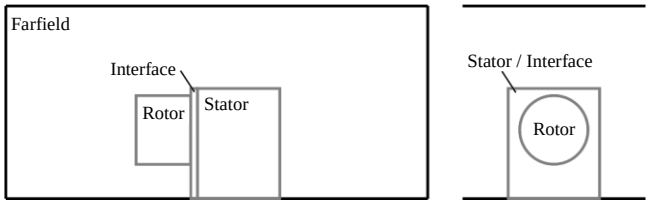

Fig. 2 Grid structure with 4 sections

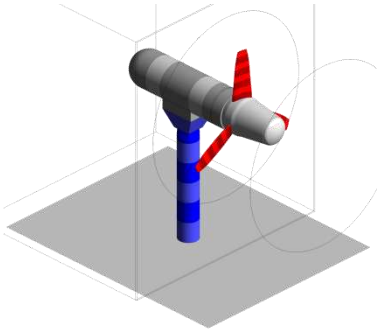

Fig. 3 Segmented surface in CFD grid for FMBI

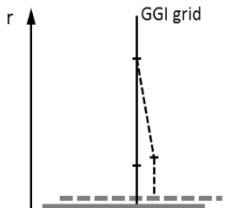

Fig. 4 Blending scheme for GGI interface grid initial (solid) and with deflection (dashed)

B. MBS-Model

The basic method of a multibody system (MBS) is to combine a discrete number of components, each described by its dynamic properties, to the dynamics of the system. In comparison to the FEM approach of discretizing the structure into a large number finite elements the MBS offers reduced computational effort on the cost of reduced level of detail in the results.

Each of the components in the multibody system is modelled using either a rigid object, a modal reduced beam or a modal reduced FEM-model. Those reduced objects are then coupled by force elements, e.g. springs, to represent the

connectivity of the components. The complete MBS model is setup in the code Simpack, [22], as shown in Fig. 5.

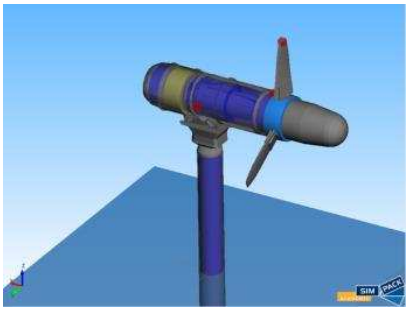

Fig. 5 MBS model of the Voith HyTide® 1000-13 Tidal Current Turbine

Table I shows the list of discrete components modelled here for the simulated Voith HyTide®1000-13 turbine. While for the rotor blades and the tower a beam model is sufficient, the nacelle housing and main shaft requires a more thorough approach. Based on the Abaqus FEM models of [13] the eigenfrequencies and modes have been simulated. These are then imported to Simpack and considered as modal degrees of freedom.

The loads on the turbine are considered based on their transients. The steady loads of gravity and buoyancy are considered being only an offset in the mean value and therefore not contributing to the hydro-elastic response of the turbine. Only the blade in-plane motion is affected by these with a 1Ω excitation. Therefore gravity and buoyancy are not taken into account.

The transient structural and hydrodynamic loads on the other side are taken into account. The structural loads like ground support, joint forces and gyroscopic loads are calculated solely in the MBS-model. The transient hydrodynamic loads like added mass, lift and drag are calculated completely in the CFD model and transferred with the FMBI algorithm.

TABLE I
MBS-MODEL

Component	Transformation	Method
Rotor blades	Modal reduced	Beam theory
Hub	Force	Rotational spring
Spinner	Rigid	Inertia tensor
Main shaft	Modal reduced	FEM
Generator	Rigid	Rotating and stationary inertia tensor
Bearings	Force	Spring
Nacelle housing	Modal reduced	FEM
Tower & transition piece	Modal reduced	Beam theory
Foundation	Force	Distributed spring along monopile
Enclosed water	Rigid	Split by location

C. FMBI-Method

As outlined above the Fluid-Structure-Interaction (FSI) is simulated within the present work with a coupled CFD-Multibody method (FMBI). The method has been developed by [4] for the coupling of Ansys CFX and Simpack as used here. It is a bidirectional and fully implicit method. It is therefore able to simulate all interactions of the turbine with the surrounding water including added mass, vortices, pressure distribution, drag, etc.

The method is based on a further discretization of the surface in the CFD grid into regions, c.f. Fig. 3, which are coupled to the corresponding body attached markers in the MBS model. Therefore the hydrodynamic loads are integrated on each of the regions and transferred to the MBS model. These loads are then used to calculate the structural response with the MBS and the deformation of the markers are transferred back to the CFD model. It is thereto required to distinguish between rigid objects and flexible objects. While for a rigid object the surface transformations on the CFD grid are homogenous, for a flexible object the transformations need to be interpolated. This is done by defining groups of flexibility in the CFD model each with a central reference curve as shown in Fig. 6. The full details of the interpolation method are presented by [4].

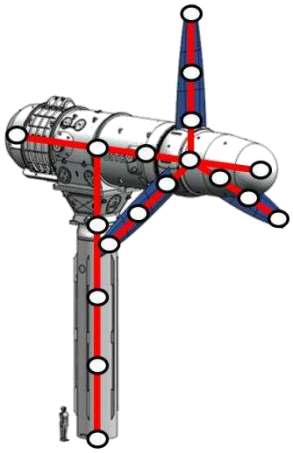

Fig. 6 Voith HyTide® turbine split into flexibility groups (solid lines); number of discrete markers (○) reduced by approx. 1/2 for visibility

For the tidal turbine areas of rigid motion are defined at the housing section above the tower and at the hub, connected by flexibility groups along each blade, along the tower and in the rear and front nacelle region. As sketched by Fig. 3 and Fig. 6, this lead to a total of 39 discrete spots of communication.

As named above the method is bidirectional and fully implicit. It therefore consists of two simulations running in parallel and communicating on each inner iteration. Subsequently the CFD grid is updated and transformed multiple times during the time step convergence with the corresponding structural integration with updated hydrodynamic loads. Each time step was chosen here to consist of at least three inner iterations (coefficient loops in CFX, time integrations in Simpack) leading to a stable and fast convergence of the results.

The FMBI method and its implementation have been verified by [4] and [8] and systematically validated by [5]. As there is no full scale data in high enough quality available to validate the present case, [5] split the issue into 3 partial

validations for the CFD, MBS and coupling methodology in separate. The validity of the standalone CFD, cf. [24], and MBS model have been discussed above. For the coupling methodology a set of free decay motions is proposed by [5]. In all test scenarios the method was able to match the numerical respectively experimental reference data within acceptable margin of measurement uncertainties. It is therefore assumed valid for the here presented investigations.

III. Operational Loads

Within this section the operational loads are analysed and the impacts of the flexibility of individual components are quantified. In order to do so an exemplary point of operation is simulated with varying complexity. A current speed of $v_1 = 4m/s$, lee orientation and a tip speed ratio in the overspeed region $\lambda_{TSR} = 8$ close to the run-away point is chosen. The rotor is therefore operating in the tower shadow and the power coefficient c_P oscillates around a small mean value. This point of operation represents the overspeed controlled turbine in a high current speed and is a typical ultimate load case scenario, [3].

With the three rotor blades of the turbine this case results in a dominant 3Ω and 6Ω excitation on the tower, hub, etc. The blades are subject to the shear and tower wake resulting in a strong 1Ω and 2Ω excitation. There is no wideband excitation of the system as in a typical stochastic load case simulation, as the inflow is uniform without turbulence. A deterministic periodic motion is therefore expected.

A. Flexible Turbine Motion

In a first step the turbine is simulated fully flexible with all components active. This resulted in the dynamic motions of the system sketched in Fig. 7. The blade tips are moving in an elliptic circle with a close to constant deflection on the upper side. On the lower side, the rotor blade reduces its deflection with the reducing shear current velocity. When entering the tower wake the blade tip swings back towards the tower and even reaches a negative deflection. However the overall deflection is with ca. $2.3cm$ at the topmost position of the blade tip quite small.

As the thrust load of the rotor is oscillating due to the tower wake a strong fore-aft-motion of the nacelle was expected. All other motions were expected to be small, as the exciting loads are small. However this was not observed in the present simulations. Instead the tower deflection was more or less constant over time with the nacelle in a bow position and a strong nodding motion. Also the nacelle is shaking on the tower torsional mode. Furthermore the nacelle is in a non-periodic side-side-motion with approx. double the amplitude of the fore-aft-motion as shown by Fig. 8.

To explain these motions they need to be distinct into 2 groups. Starting with the nacelle nodding and shaking motion, they are clearly a result of the 3Ω excitation due to the tower wake. This 3Ω excitation at $f_{3\Omega} = 2.35Hz$ is a significantly higher frequency than the 1st tower eigenfrequency, cf. Fig. 18, and subsequently the nacelle fore-aft-motion is not able to follow the loading and the amplitude is reduced. The 2nd bending eigenfrequency as well as the torsional eigenfrequency on the other hand are close or higher than the the 3Ω. In combination with the tower shadow causing not only an oscillating rotor thrust, but also a time dependent side loading in the rotor plane and a periodic nodding moment, the present motion occurs.

The source for the non-periodic nacelle side-side motion Δy, cf. Fig. 8, on the other hand is not a result of the rotor loadings. A frequency domain analysis of Δy results in the frequencies $f = 2.37Hz$ and $f = 1.51Hz$. The first is approx. the 3Ω excitation, the latter is the vortex shedding frequency on the tower. The turbine is therefore in a vortex induced motion state combined with the 3Ω oscillation.

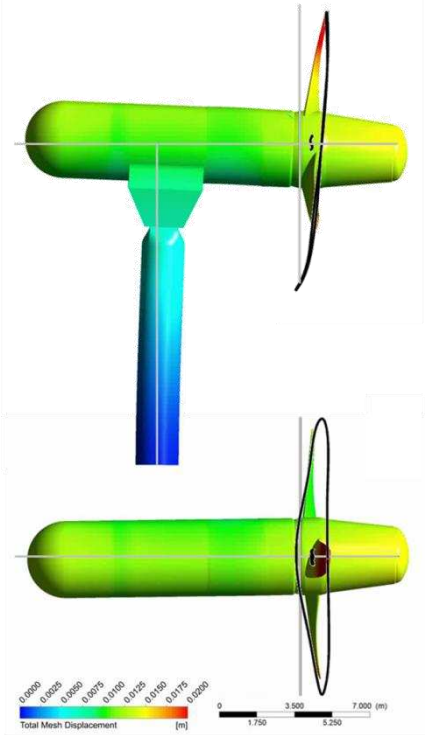

Fig. 7 Fully flexible turbine during periodic motion coloured by displacement - Grey lines denote the undeformed central reference curves, Black lines denote motion of blade tip resp. hub center over time. (Deformations scaled by 50 for visibility)

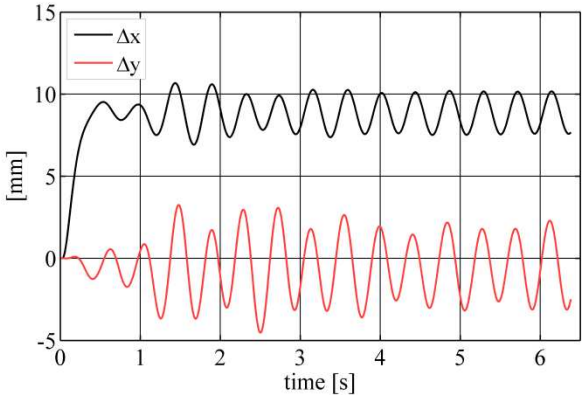

Fig. 8 Tower top motion over time - only tower flexible here (Table II, case V - fully flexible case is equivalent but not started from zero deflection)

B. Simulated Configurations

As given above the core question of this research is to identify the relevant components for the hydro-elastic behaviour of the turbine. Therefore the structural model is varied and a total of 10 different setups were simulated. These are listed in Table II.

As the time required for the onset of the oscillation depends on the actual setup, e.g. approx. 3.5 revolutions for case V shown in Fig. 8, the simulated number of revolutions was adapted. The main purpose of this was to reduce the required computational resources to an acceptable limit. While e.g. case III took only a single revolution till convergences starting from the rigid solution, the fully flexible case took three additional revolutions starting from the converged result of case VII. The fully flexible case therefore was simulated e.g. for five revolutions taking approx. 160h on 20Cores, 2.2GHz.

This method did not change the results, however bringing the two frequencies observed above to mind, the phase angle between rotor revolution and vortex shedding on the tower is time dependent. Subsequently, as the described method of using other cases as initial conditions also appends the absolute time of the simulations, the relative phase position of the two load oscillations changes with each case. Therefore the forces from the vortex induced motion differ on each simulation and the loads on the turbine may differ slightly on the direct comparison due to this effect. Also the results are not any more exact 3Ω periodic as initially expected, but vary slightly between each blade passage, as can be seen e.g. in Fig. 9 comparing the values at 240° and 360°. Nevertheless this inconvenience was considered well worth the reduced computational effort.

TABLE II
NUMBER OF EIGEN-MODES IN EACH SIMULATED COMBINATION

Case	Main shaft	Nacelle housing	Blade	Tower & Ground*	Transition piece
Rigid					
I	3				
II	3	4			
III			3		
IV	3	4	3		
V				6	
VI				5	
VII				5	3
VIII			3**		
Fully flexible	3	4	3	5	3

*) 5: tower torsional rigid at seabed; 6: ground torsional soft
**) blade out-of-plane eigenfrequency in air reduced by 50%

C. Variation of Drivetrain Flexibility

The first set of comparisons of flexibility variations is done for the drivetrain and nacelle components (case I…IV). Fig. 9 compares the axial thrust force on the hub $F_{x\,Hub}$ during the passage of 1 blade at the tower. There is close to no impact to this load due to the drivetrain flexibility. As the nacelle (case II) and shaft (case I) are both very stiff in this direction their impact was expected to be small. The out-of-plane bending mode of the rotor blade (case III) on the other hand has a higher impact to $F_{x\,Hub}$. However, the blade out-of-plane eigenfrequency is much larger than the excitation $f_{OoP\,Blade} \gg 1\Omega$ and subsequently the impact can be neglected. This result is specific for the here investigated geometry and might change for other blade designs as will be discussed below.

For the hub torque $Q_{x\,Hub}$ the impact of the drivetrain flexibility is larger, Fig. 10. Depending on the combinations of flexibility the hub is oscillating in a rotating mode. In case III the blades are flexible and oscillating in the in-plane eigenfrequency. This oscillation has a low damping ratio and is subsequently oscillating over a large number of periods. As the shaft and hub are rigid and rotating with a constant speed each blade mode is uncoupled from the other blades.

In case I/II the rotor is now rigid and the oscillation is on the shaft. Subsequently the momentum introduced by the tower shadow to the blade is spread amongst the rotor and therefore the oscillation is smaller.

Also with case IV, which is the combination of II and III, the shaft is no more rigid and the blade modes are no more uncoupled. In the same way as for case II the momentum to the blade is spread amongst the 3 rotor blades and the in-plane oscillation is reduced.

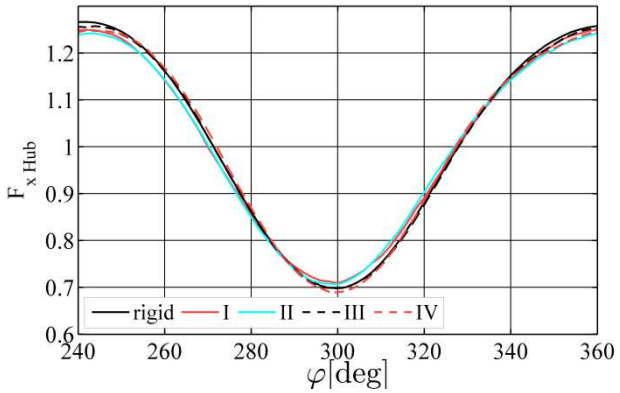

Fig. 9 Axial hub force $F_{x\,Hub}$ with varying drivetrain flexibility normalised with mean value $\bar{F}_x|_{rigid}$

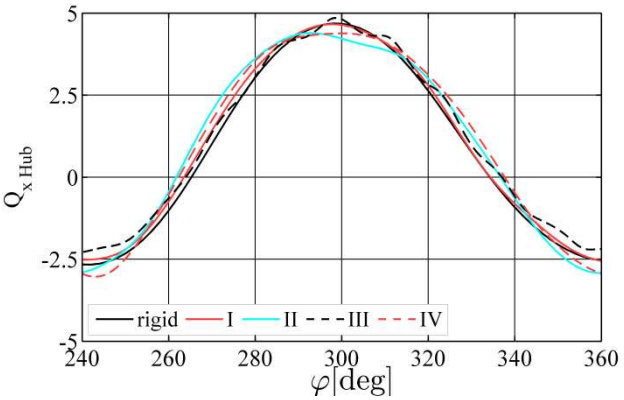

Fig. 10 Hub torque $Q_{x\,Hub}$ with varying drivetrain flexibility normalised with mean value $\overline{Q_x}|_{rigid}$

Fig. 11 shows the impact of the drivetrain flexibility to the tower bottom bending moment $M_{y\,TowerBottom}$. As can be seen the rotor blade and main shaft have a minor effect. The nacelle on the other hand has a significant impact to tower bottom bending moment. While the impact of the rotor thrust to $M_{y\,TowerBottom}$ maintains the same, cf. Fig. 9, the nodding moment of the rotor is no more transmitted in its full extend through the nacelle into the tower top.

As the 6Ω frequency is in the same magnitude as the nacelle nodding eigenfrequency there is an additional eigenmotion on this frequency. Subsequently the amplitude of $M_{y\,TowerBottom}$ is reduced but it gets a strong 6Ω component visible in the two additional extremal points.

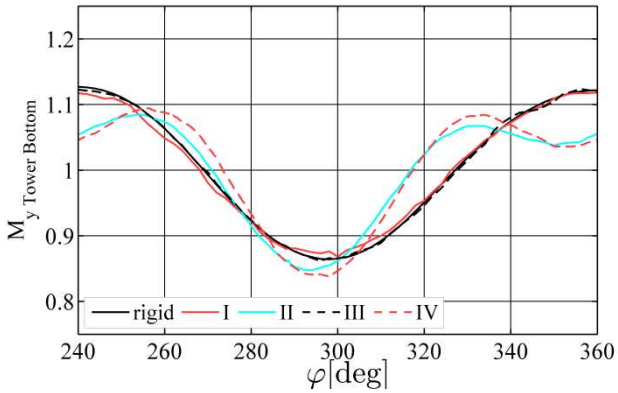

Fig. 11 Tower bottom bending moment $M_{y\,TowerBottom}$ with varying drivetrain flexibility normalised with mean value $\overline{M_y}|_{rigid}$

D. Variation of Blade Flexibility

As outline initially most research on hydro-elasticity on tidal current turbines focuses on the rotor blade out-of-plane mode as done in the wind energy state of the art. However, in the present simulations this flexibility was of negligible impact, which might be the result of the specific design of the Voith HyTide®1000-13 rotor blades. Fig. 12 shows the comparison to a theoretic rotor blade (case VIII) with the blade stiffness reduced by factor of four. On a real blade this would be achieved by reducing the thickness of the blade by a factor of $\sqrt[3]{1/4} \approx 0.63$, but for simplicity the same blade surface geometry is used.

It needs to be mentioned that it is doubtful whether a rotor blade with these parameters could operate safely or would crack. However, for the present comparison it can be used to identify the impact.

Maintaining the blade mass the stiffness reduction reduced the eigenfrequency in air by 50%. Despite the eigenfrequency is still 6 times larger than the dominant 1Ω excitation the impact of the rotor blade flexibility to $F_{x\,Hub}$ is much larger. The amplitude of this load is significantly increased due to the large mass of blade oscillating with large amplitude.

The rotor blade therefore needs to be checked weather its specific design has an impact or not. For the present case of the Voith HyTide®1000-13 turbine it can be neglected.

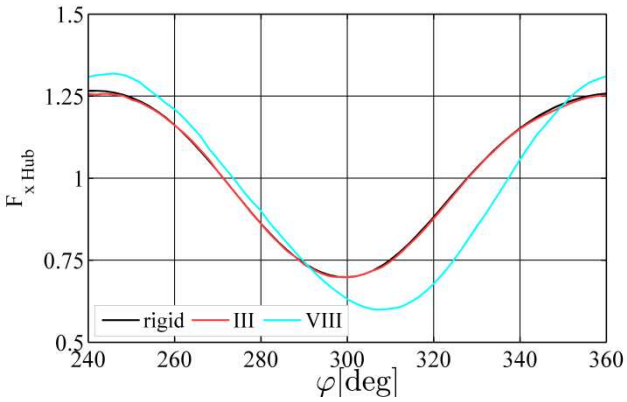

Fig. 12 Axial hub force $F_{x\,Hub}$ with reduced blade stiffness normalised with mean value $\overline{F_x}|_{rigid}$

E. Variation of Structure Flexibility

The 2nd big group of flexibility variations are the tower and ground flexibility. Starting with the driving torque at the hub $Q_{x\,Hub}$, Fig. 13, there is only a small impact noticeable. Despite this impact is larger than any observed for the drivetrain flexibility variations, it is mainly a phase shift. This phase shift occurs due to the nodding motion of the turbine and the subsequent fore-aft motion of the outer blade sections, influencing the torque values.

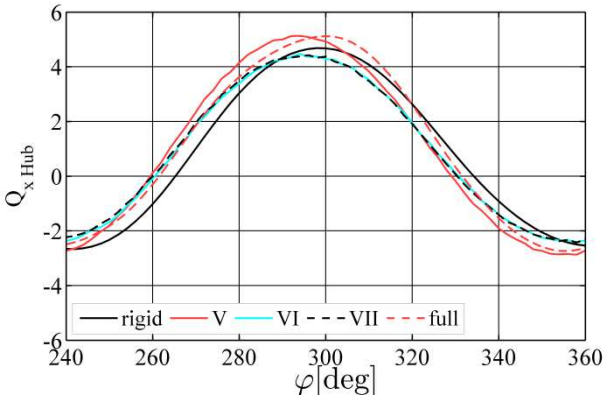

Fig. 13 Hub torque $Q_{x\,Hub}$ with varying structure flexibility normalised with mean value $\overline{Q_x}|_{rigid}$

For the axial load on the hub $F_{x\,Hub}$ there is a more severe impact, Fig. 14. On one hand the lift values on the rotor blades are influenced as described for $Q_{x\,Hub}$, on the other hand the nacelle is in a fore-aft-motion. This motion is small as shown above, cf. Fig. 8, however due to the high frequency and mass of the rotor and hub system the resultant momentum loads $F = m \cdot a$ are of relevant size. Therefore the amplitude of $F_{x\,Hub}$ is reduced by approx. 30%.

It is an interesting correlation, that the drivetrain flexibility (case 'full'), which had isolated near to no impact to this value, cf. Fig. 9, now reduces the impact of the structure flexibility to this load. The exact reason for this is still under investigation but is most probably a result of the nodding flexibility of the housing as discussed in Fig. 11.

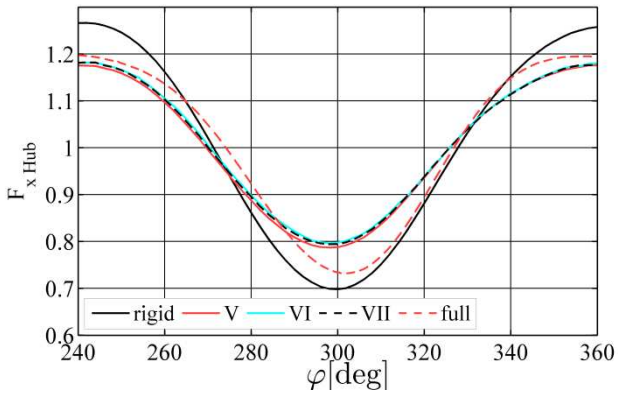

Fig. 14 Axial hub force $F_{x\,Hub}$ with varying structure flexibility normalised with mean value $\overline{F_x}|_{rigid}$

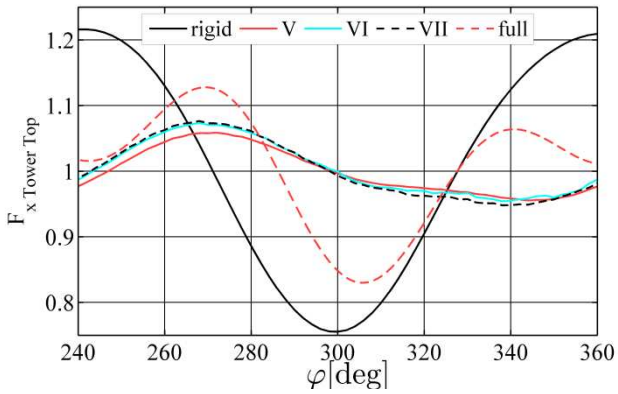

Fig. 15 Axial tower top load $F_{x\,TowerTop}$ with varying structure flexibility normalised with mean value $\overline{F_x}|_{rigid}$

The latter claim is also supported by the axial tower top load $F_{x\,TowerTop}$, Fig. 15. Here the same results as for the hub loading can be found, however the impact of the inertia is significantly stronger. The amplitude of the load is now reduced by approx. 70% due to the high mass of the nacelle unit with the included water. Including also the drivetrain flexibility (case full) the nodding mode of the nacelle results in a 6Ω load variation on the $F_{x\,TowerTop}$. Also as for the $F_{x\,Hub}$ the load amplitude is not as strong reduced as with only the structure flexible.

Comparing the cases V and VI they differ in their treatment of the torsional rigidity of the ground. While VI treats the ground torsional stiff, V is torsional soft and subsequently they differ in their results on the nacelle shaking motion. Fig. 16 shows the tower top torsional moment $M_{z\,TowerTop}$. As can be seen including the torsional flexibility of the tower increases the load amplitude compared to the rigid case. Especially in case V the loads are significantly higher. This is a result of the lower stiffness of the system and subsequent higher motion amplitudes in V. The transition piece (case VII) and the drivetrain respectively nacelle flexibility (case full) are of minor importance here.

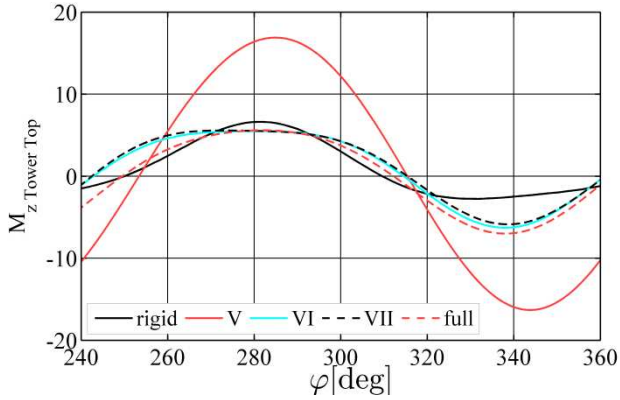

Fig. 16 Tower top torsional load $M_{z\,TowerTop}$ with varying structure flexibility normalised with mean value $\overline{M_z}|_{rigid}$

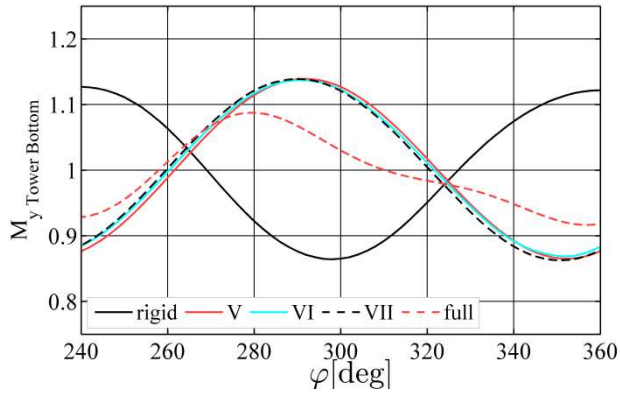

Fig. 17 Tower bottom bending moment $M_{y\,TowerBottom}$ with varying structure flexibility normalised with mean value $\overline{M_y}|_{rigid}$

For the tower bottom bending moment $M_{y\,TowerBottom}$, Fig. 17, the tower flexibility results in approx. the same load amplitude as in the rigid case, however the phase is shifted by approx. $\theta = 0.87 \cdot \pi$. As the tower eigenfrequency is significantly smaller than the 3Ω excitation this phase shift is the expected result, cf. Fig. 18.

Based on those findings it can be concluded that for the present load case the tower and the housing flexibility are of significant impact for the loads. The other flexibilities are relevant for some specific loads, but have minor impact to the overall hydro-elastic behaviour of the turbine.

F. Impact of Point of Operation

At multiple occasions above the relativity of excitation frequency and eigenfrequencies has been mentioned. Following this path a large impact of the point of operation can be noted. Therefore the present investigation is not conclusive but needs to be extended to other points of operation in future. Especially the operation in a point of resonance of any component might reveal different result.

Assuming a 1DoF oscillator the resonance behaviour could be extrapolated with a Bode-diagram as shown in Fig. 18 for $M_{y\,TowerBottom}$ in case V by fitting the observed load amplitude and phase shift θ. However, this is only an

extremely coarse approximation of the loads and not suitable for design calculations. Only with high fidelity simulations in the point of resonance the loads can be calculated adequately.

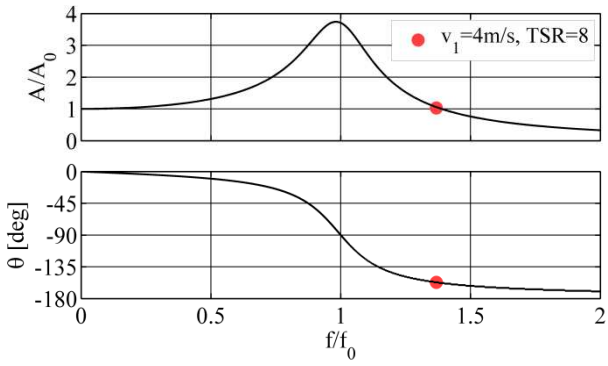

Fig. 18 Resonance load amplification extrapolated for $M_{y\,TowerBottom}$

Therefore the next step within this research will be the extension to a Bode-diagram of FSI simulations for different current speeds and speeds of revolution. Also stochastic turbulent inflow conditions might be taken into account for further investigation. However, this will massively increase the numerical effort.

IV. Conclusions

The present paper investigated the impact of flexibility to the hydro-elastic behaviour of a tidal current turbine and tried to answer, which components are relevant for the hydro-elastic behaviour of the tidal current turbine. To do so a fluid-multibody-interaction model based on coupled CFD and multibody dynamics has been setup and simulated in an exemplary point of operation. A total of 10 different cases with varying combinations of component flexibilities have been simulated for the Voith HyTide®1000-13 turbine.

These cases are then compared and the impact to the loads on key locations within the turbine is evaluated. Based on the results it was found, that the flexibility of the rotor blades and main shaft are of minor importance. The hydro-elastic behaviour and loads of the turbine are dominated by the tower fore-aft bending and the nacelle nodding properties.

Therefore for simplified models and stochastic load simulations the blade and shaft flexibility may be neglected and only the tower and nacelle eigenmodes need to be taken into account.

The paper concluded with an outlook to the point of operation, which will further amplify the impact of each component.

Acknowledgment

This research has been conducted within a joint project of Stuttgart Wind Energy, University Stuttgart, and Voith Hydro Ocean Current Technologies GmbH & Co. KG. Further it is supported by the software suppliers Simpack AG and Ansys Germany GmbH.

References

[1] Ansys “CFX Theory Guide v14.5”, Code documentation, 2013

[2] M. Arnold, F. Biskup, D. Matha “Untersuchung einer Gezeiten-strömungsturbine und Haltestruktur mittels strömungsmechanischer Simulation“, thesis, University Stuttgart, Germany, Okt. 2011

[3] M. Arnold, F. Biskup, P.W. Cheng “Simulation of Rotor-Foundation-Interaction on Tidal Current Turbines with Computational Fluid Dynamics”, 10th EWTEC 2013, Aalborg, Denmark

[4] M. Arnold, F. Biskup, P.W. Cheng “Simulation of Fluid-Structure-Interaction on Tidal Current Turbines Based on Coupled Multibody and CFD Methods”, Journal of Ocean and Wind Energy (JOWE), Vol. 1, No. 2, pp. 119-126, May 2014

[5] M. Arnold, M. Kretschmer, F. Biskup, J. Koch, P.W. Cheng “A Validation Method for Fluid-Structure-Interaction Simulations Based on Submerged Free Decay Experiments”, 25th ISOPE 2015, Kona, USA

[6] M. Arnold, F. Biskup, P.W. Cheng “Load Reduction Potential of Variable Speed Control Approaches for Fixed Pitch Tidal Current Turbines”, 11th EWTEC 2015, Nantes, France

[7] K. Bercin, T. Lloyd, Z.-T. Xie, S. Turnock “Efficient method for analyzing fluid-structure interaction of horizontal axis tidal turbine blades”, 10th EWTEC 2013, Aalborg, Denmark

[8] F. Beyer, M. Arnold, P.W. Cheng “Analysis of Floating Offshore Wind Turbine Hydrodynamics using coupled CFD and Mulitbody Methods”, 23rd ISOPE 2013, Anchorage, USA

[9] C. Faudot, O. Dahlhaug, M. Holst “Tidal turbine blades in runaway situation: experimental and numerical approaches“, 10th EWTEC 2013, Aalborg, Denmark

[10] Garrad Hassan “Tidal Bladed – Theory Manual”, 2015

[11] C.-H. Jo, D.-Y. Kim, Y.-H. Rho, K.-H. Lee, C. Johnstone “FSI analysis of deformation along offshore pile structure for tidal current power“, Journal of Renewable Energy, Vol. 54, pp. 248-252, June 2013

[12] B.-S. Kim, S.-Y. Bae, M.-K. Kim, W.-J. Kim, S.-L. Lee “Performance Prediction and Structural Integrity Assessment of 50-kW Tidal Turbine Using Unidirectional FSI Method“, 22nd ISOPE 2012, Rhodes, Greece

[13] G. Kreuzwirth, T. Resch “Rotor Dynamic and Bearing Analysis of an Instream Tidal Energy Converter”, AVL, Report CC0494, July 2012

[14] F. Lippold, E. Ohlberg, A. Ruprecht “Partitioned Fluid-Structure Coupling and Vortex Simulation on HPC-Systems” in “High Performance Computing in Science and Engineering ‘08”, ISBN 978-3-540-88301-2, Springer, Germany, 2009

[15] D. Matha, S.-A. Fischer, S. Hauptmann, P.W. Cheng, D. Bekiropoulos, T. Lutz “Variations in Ultimate Load Predictions for Floating Offshore Wind Turbine extreme Pitching Motions applying different Aerodynamic Methodologies“, 23rd ISOPE 2013, Anchorage, USA

[16] C. Morris “Influence of Solidity on the Performance, Swirl Characteristics, Wake Recovery and Blade Deflection of a Horizontal Axis Tidal Turbine”, PhD-thesis, Cardiff University, England, 2014

[17] J. N. Newman “Marine Hydrodynamics“, ISBN 978-0-262-14026-3, MIT Press, USA, 1977

[18] R. Nicholls-Lee “Adaptive Composite Blades for Horizontal Axis Tidal Turbines“, PhD-thesis, University of Southampton, England, 2011

[19] T. O’Doherty “Optimising Tidal Stream Turbine Performance: Modelling”, LCRI Annual Conference 2013, Llandudno, Wales

[20] S.W. Park, S. Park, S.H. Rhee “Performance Predictions of a Horizontal Axis Tidal Stream Turbine Considering the Effects of Blade Deformation”, 3rd International Symposion on Marine Propulsors, smp’13, Launceston, Australia, 2013

[21] C. Sickinger “Assessing the Effect of Composite Blades in the Development of 1MW Tidal Turbines“, 32nd ACUM 2014, Nürnberg, Germany

[22] Simpack “Simpack Documentation v9.5“, Code documentation, 2013

[23] R. Starzmann, M. Baldus, E. Groh, N. A. Lange, S. Scholl “Full-Scale Testing of a Tidal Energy Converter Using a Tug Boat“, 10th EWTEC 2013, Aalborg, Denmark

[24] Voith “EMEC Load Assessment EMEC01“, Voith Report 2-01052203, Jan. 2015

[25] Y. Young, M. Motley, R. Yeung “Three-Dimensional Numerical Modeling of the Transient Fluid-Structural Interaction Response of Tidal Turbines”, Journal of Offshore Mechanics and Arctic Engineering, Vol. 132, No. 1, Feb. 2010